Does the Wind Control the Import and Export of the South Atlantic?

DORON NOF*

Department of Oceanography, The Florida State University, Tallahassee, Florida

(Manuscript received 17 May 1999, in final form 9 December 1999)

ABSTRACT

A different way of examining the meridional flux of warm and intermediate water ($\sigma_\theta < 27.50$) from the Southern Ocean into the South Atlantic is proposed. The method considers the Americas to be a ''pseudo island'' in the sense that the continent is entirely surrounded by water but has no circulation around it. It is shown that, although the northern connection between the Atlantic and the Pacific (via the Bering Strait) is weak, it imposes severe limitations on the sea level in the Atlantic basin: so much so that it allows one to compute the meridional transport without finding the detailed solution to the complete wind–thermohaline problem. The method employs an integration of the linearized momentum equations along a closed contour containing the Americas, Greenland, the Atlantic, and parts of the Arctic Ocean.

First, an idealized rectangular model involving three layers, an active continuously stratified upper layer containing both thermocline ($\sigma_\theta < 26.80$) and intermediate water ($26.80 < \sigma_\theta < 27.80$), an inert deep layer ($27.80 < \sigma_\theta < 27.90$), and a southward moving bottom layer ($\sigma_\theta > 27.90$) is considered. In this idealized model, the Americas are represented by the pseudo island. Deep-water formation is allowed (in the northern part of the basin east of the Americas and south of the gap connecting the Atlantic–Arctic basin to the Pacific), but the cooling rate need not be specified. The basin is subject to both zonal winds and heat exchange with the atmosphere [i.e., $\rho = \rho(x, y, z)$], but, for simplicity, (temporarily) meridional winds are not allowed. A simple analytical expression for the transport of the meridional overturning cell is derived, and process-oriented numerical experiments that were conducted (using a primitive equation layer-and-a-half isopycnic model) are in excellent agreement with the theory.

The theory is then extended to a more convoluted geography subject to both zonal and meridional winds. The surprising result is found that, even for the complex situation, the northward transport of upper and intermediate water is given simply by $\oint \tau^l \, dl/\rho/f_0$, where f_0 is the average Coriolis parameter along a line connecting the southern tip of the Americas with the southern tip of Africa and τ^l is the wind stress along the integration path (l). This implies that, although the amount of high-latitude cooling is responsible for the location and manner in which bottom water is formed, it has very limited effect on the net meridional mass flux (which constitutes the so-called conveyor).

Detailed application of the above formula to the Atlantic using actual geography and spherical coordinates as well as actual meridional and zonal winds (adopted from 40-yr averages given by NCEP) gives the reasonable estimate of 9 Sv (Sv $\equiv 10^6$ m^3 s^{-1}) for the transport of the conveyor upper limb.

1. Introduction

The South Atlantic is the conduit for upper ocean water that flows northward and ultimately sinks in the North Atlantic, forming the North Atlantic Deep Water (NADW). Understanding the meridional flux in the South Atlantic is, therefore, of direct relevance to the earth's climate.

According to conventional wisdom, this meridional transport and the ultimate production of NADW is primarily due to atmospheric cooling (with the wind playing a secondary role). In line with this logic, direct wind action and thermohaline processes have, traditionally, been studied independently from each other (assuming that they also *act* independently of the other). It has never been demonstrated, however, that the two processes are, in fact, independent. We shall demonstrate in this paper that not only are the two not necessarily independent but, in our particular case, it is the wind field, rather than the cooling, that is the main agent controlling the amount of water that enters the South Atlantic from the Southern Ocean.

We shall consider the question of how much water flows northward from the Southern Ocean into the South Atlantic in terms of a wind-driven intergyre exchange process subject to atmospheric cooling. The exchange is taking place in an (Atlantic) basin separated from the

* Additional affiliation: Geophysical Fluid Dynamics Institute, The Florida State University, Tallahassee, Florida.

Corresponding author address: Dr. Doron Nof, Department of Oceanography 4320, The Florida State University, Tallahassee, FL 32306-4320.
E-mail: nof@ocean.fsu.edu

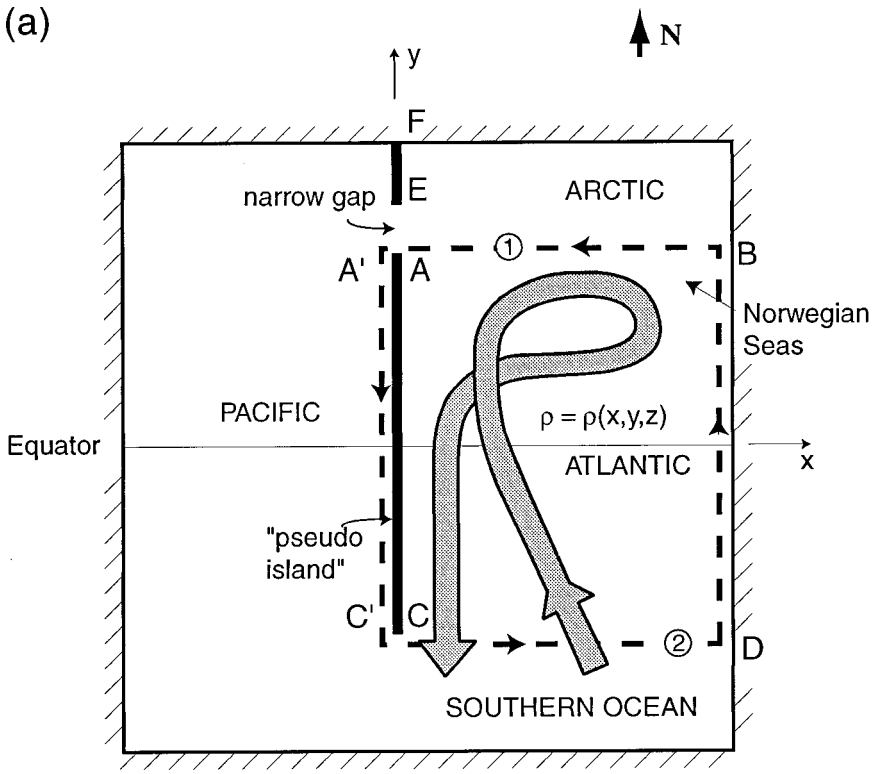

FIG. 1a. Top view of the simplified meridional flow model. (This model with a rectangular basin is hereafter referred to as the first model.) Here, the Atlantic and Arctic Oceans are connected to the Pacific via a narrow gap (representing the Bering Strait) that allows the equalization of pressures across it but is too narrow to allow significant flow through it. With this simple geometry (which is used merely for the clarity of the presentation) the thermocline and intermediate water are driven northward by zonal winds and thermohaline processes. Sinking occurs south of **AB**. An inert deep layer is sandwiched between the northward flowing surface water and the southward flowing bottom water. Actual calculations for the Atlantic were done using a more realistic model that takes into account the appropriate geography of the continents, the sphericity of the earth, and meridional winds. (This more realistic model will later be referred to as the second model.) The thick broken line (which passes on to the left-hand side of the pseudo island) denotes the closed integration path. Points **A** and **A′** (as well as **C** and **C′**) correspond to the eastern and western edges of the continent northern (southern) tip.

(Pacific) basin by a ''pseudo island'' representing the Americas. By ''pseudo island'' we mean a continent surrounded partly by open water and partly by a channel containing nearly stagnant water (see Fig. 1).

Our approach is different than that usually taken in that it involves integration of the linearized momentum equations over the pseudo island and the ocean to the east of the continent. The nearly stagnant channel is crucial to our problem because it ''equalizes'' the pressures on the northern parts of the pseudo island in the sense that it forces the pressure to be continuous around the continent. The density is allowed to vary in space and all waters that enter the South Atlantic are required to sink in the North Atlantic. Hence, thermohaline processes are represented by the varying density and the deep-water formation. Antarctic Bottom Water (AABW) is not excluded from the model in the sense that both localized as well as distributed exchange between the deep and intermediate ocean is allowed. However, our final estimate of 9 Sv (Sv $\equiv 10^6$ m^3 s^{-1}) for the meridional overturning cell (MOC) transport does not include AABW entering the Atlantic from the south.

We shall see that the equalization of the pressure by the Bering Strait has a far-reaching effect on the flow field. Due to this equalization and the associated continuity of pressure around the continent, the MOC transport can be computed from the wind field, the geography, and the general location of the NADW formation. Namely, we shall demonstrate that it is not necessary to solve the complete wind–thermohaline problem in order to compute the transport of the MOC.

a. Background

Gordon (1986) was the first to suggest that the transport of the upper conveyor limb (which ultimately sinks

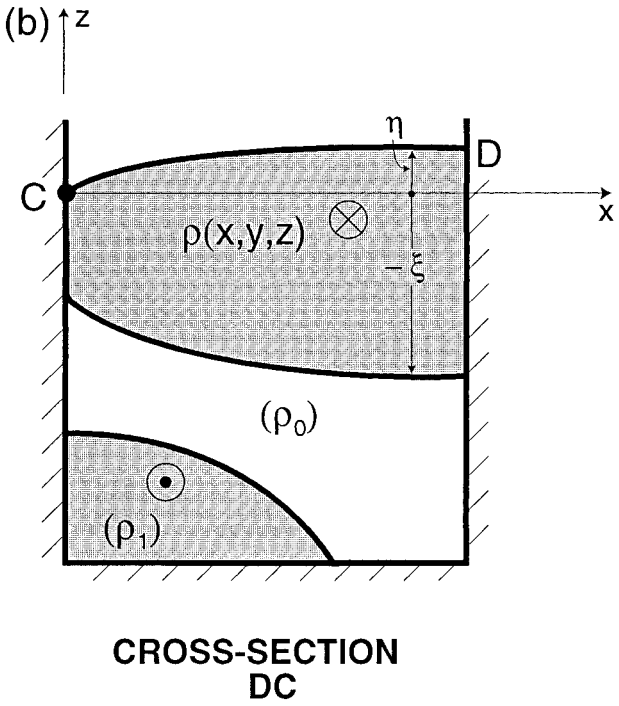

FIG. 1b. A cross section of the first model [shown in (a)]. The upper water [$\rho = \rho(x, y, z)$] corresponds to thermocline water as well as intermediate water (i.e., all waters with a density less than $27.80\sigma_\theta$). The stagnant deep water (ρ_0) corresponds to $27.80 < \sigma_\theta < 27.90$. Both the free surface vertical displacement η and the lower interface displacement ξ are measured positively upward from $z = 0$.

in the North Atlantic) enters the upper South Atlantic near the tip of South Africa. Specifically, he proposed that warm water enters the South Atlantic mostly due to the influx of Agulhas rings. These rings are relatively large (~500 km in diameter) and deep (~800 m) and have been observed to drift westward at rates of 5–8 cm s^{-1} (Olson and Evans 1986).

Using inverse calculations, Rintoul (1991) disputed Gordon's (1986) arguments and suggested that the origin of the upper conveyor limb (i.e., the water that ultimately sinks in the North Atlantic) is the Drake Passage rather than the tip of South Africa (suggested by Gordon). He proposed that this cold water route accounts for roughly 17 Sv, which is equally split among surface, intermediate, and bottom water. In a subsequent article, Gordon et al. (1992) proposed a circulation pattern somewhat different from both Gordon's (1986) original suggestion and Rintoul's (1991) flow pattern. In their new scenario, much of the Indian Ocean surface water that enters the South Atlantic (via the Benguela Current and Agulhas rings) recirculates and exits the South Atlantic. Furthermore, the 10 Sv or so that, in their opinion, does cross the Atlantic equator consists mainly of intermediate rather than surface water. According to Gordon et al. (1992) this intermediate water originates in the Drake Passage and loops in the Indian Ocean before entering the Atlantic.

Saunders and King (1995) have used recent World Ocean Circulation Experiment data to argue that as originally suggested by Gordon (1986), about 10 Sv of mainly surface water enters the South Atlantic along the warm water path. Schmitz (1996) also suggests such a warm water route. Recent numerical computations (Barnier et al. 1998; Marchesiello et al. 1998) suggest, on the other hand, that the overturning cell consists mainly of cold, rather than warm, water. These numerical calculations point to a transport of 16 Sv, which is in agreement with the recent hydrographic estimates of Schlitzer (1996). They are also consistent with Matano and Philander's (1993) calculations showing a conversion of intermediate to surface water in the South Atlantic. The reader is also referred to Drijfhout et al. (1996) where other aspects of this circulation are discussed. The reader is warned, however, that all of these model studies drive their overturning via their (specified) boundary conditions or choose (implicitly or explicitly) a mixing parameterization that determines the overturning so that, in a way, they do not add much to the above disagreement.

Our new analytical technique will show that upper water (i.e., thermocline and intermediate water corresponding to $\sigma_\theta < 27.50$) can be forced northward across the equator only if there are significant interhemispheric asymmetries in the wind field and the geography. It turns out that the asymmetry in the geography and the observed wind field above the Atlantic allow for about 9 Sv of upper and intermediate water to be transported meridionally. Sixty percent of this transport is due to the (strong) southern winds.

b. Present approach

Consider first the idealized ocean shown in Figs. 1 and 2. This simplified configuration (hereafter referred to as the ''first model'') is sufficient for illustrating the essence of the problem and is used here merely for the clarity of the presentation. Actual calculations will be done with a more realistic geography (hereafter referred to as the ''second model,'' Fig. 3). We shall consider the familiar vertically integrated equations of motion corresponding to an ocean whose interior obeys Sverdrup dynamics (section 2). Dissipation occurs underneath the swift western boundary current (WBC) as a result of interfacial friction. Cross-equatorial flow occurs via the WBC where the relative vorticity created by the meridional displacement of the fluid is immediately destroyed via friction. Some nonlinearity is contained in the model through the pressure terms (which allow large vertical displacement of the interface) but the inertial terms are neglected.

The common demand that, in a closed basin, the WBC transport be equal and opposite to that of the interior is relaxed so that a net meridional flow out of the region of interest is allowed. Such a net transport is, in general, a result of a combined interior and WBC fluxes. With

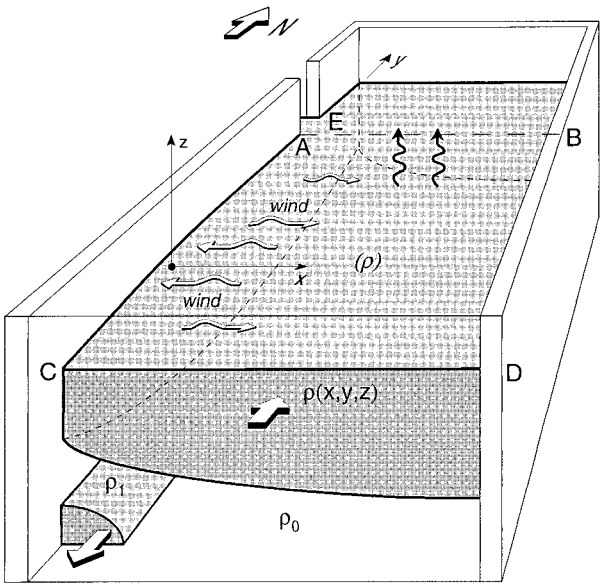

FIG. 2. A three-dimensional view of the first model (shown in Figs. 1a and 1b). Open ''wiggly'' arrows denote surface wind, open straight arrows denote transports, and solid wiggly arrows denote the cooling. Note that, in this first model, sinking and NADW formation take place in latitudes lower than the gap.

the aid of these considerations, and an integration along a closed path connecting the tips of the Americas, we shall analytically derive a formula that allows the computation of the meridional interhemispheric transport from the wind field. We shall see that this meridional transport includes flows due to *both wind and diabatic* processes.

Integration of the governing equations across the ocean and around islands is, of course, not new and was considered earlier by various authors such as Parsons (1969), Veronis (1973), Godfrey (1989), Pedlosky et al. (1997), and Pratt and Pedlosky (1998). What is new is (i) the choice of our particular closed integration path, (ii) the recognition that the connection of Atlantic water to Pacific water (via the Arctic Ocean and the Bering Strait) is crucial to the problem, and (iii) the recognition that cooling processes can only enter the problem through the pressure terms (which integrate to zero in our case) and through the location where the deep-water formation occurs.

After presenting the transport formula for the first model and illustrating the essence of the problem (section 2), we shall proceed and extend the transport formula to the more realistic second model shown in Fig. 3 (section 3). In this latter context, we shall include the following:

1) meridional winds,
2) the sphericity of the earth, and
3) the actual geometry of the boundaries.

This is followed by presenting process-oriented numerical experiments (section 4) and comparing them to our transport formula for the rectangular ocean (the first model). Some discussion of the results is included throughout the presentation; the application to the Atlantic is presented in detail in section 5 and a summary is given in section 6.

The above approach is related to Nof and Van Gorder's (1999, hereafter referred to as NVG) recent derivation of the ''separation formula'' and its application to the Atlantic. The two approaches are similar in the sense that in both cases a particularly convenient integration path is used. However, they are very different in three aspects. First, the present model has a pseudo island whereas the NVG has a separating WBC. Second, the separation formula is a *prognostic* rule whereas the pseudo island rule is *diagnostic.* This is so because the separation formula relies on input from observations (of the separation latitudes location). Third, here in the pseudo island calculation we speak about the meridional flow of *both thermocline and intermediate water* whereas the former addresses merely *thermocline water* and its associated upwelling.

2. The rectangular model

a. Governing equations

Consider again our first model (Fig. 1). The upper moving layer contains both thermocline and intermediate water. It is continuously stratified [$\rho = \rho(x, y, z)$] and is subject to both zonal wind action and heat exchange with the atmosphere. The familiar linearized Boussinesq equations are

$$-fv = -\frac{1}{\rho_0}\frac{\partial P}{\partial x} + \frac{1}{\rho_0}\frac{\partial \tau^x}{\partial z} \tag{2.1}$$

$$fu = -\frac{1}{\rho_0}\frac{\partial P}{\partial y} + \frac{1}{\rho}\frac{\partial \tau^y}{\partial z} \tag{2.2}$$

$$\frac{\partial u}{\partial x} + \frac{\partial v}{\partial y} + \frac{\partial w}{\partial z} = 0 \tag{2.3}$$

$$\frac{d\rho'}{dt} = k\nabla^2\rho', \tag{2.4}$$

where u, v, and w are the velocities in the x, y, and z directions (here, x is pointing eastward and y is pointing northward); f is the Coriolis parameter (varying linearly with y); ρ_0 the uniform density of the motionless deep water; P is the deviation of the hydrostatic pressure from the pressure associated with a state of rest; τ^x is the stress in the x direction; and τ^y is the meridional stress. (Note that our conventional notation is defined both in the text and in the appendix.) The density deviation ρ' is given by $\rho - \rho_0$ and k is the diffusion coefficient, which, as we shall see, need not be specified. [Equation (2.4) is included merely for completion; it will not be used in our analysis.] Friction will only be included in the y momentum equation on the ground that it will only

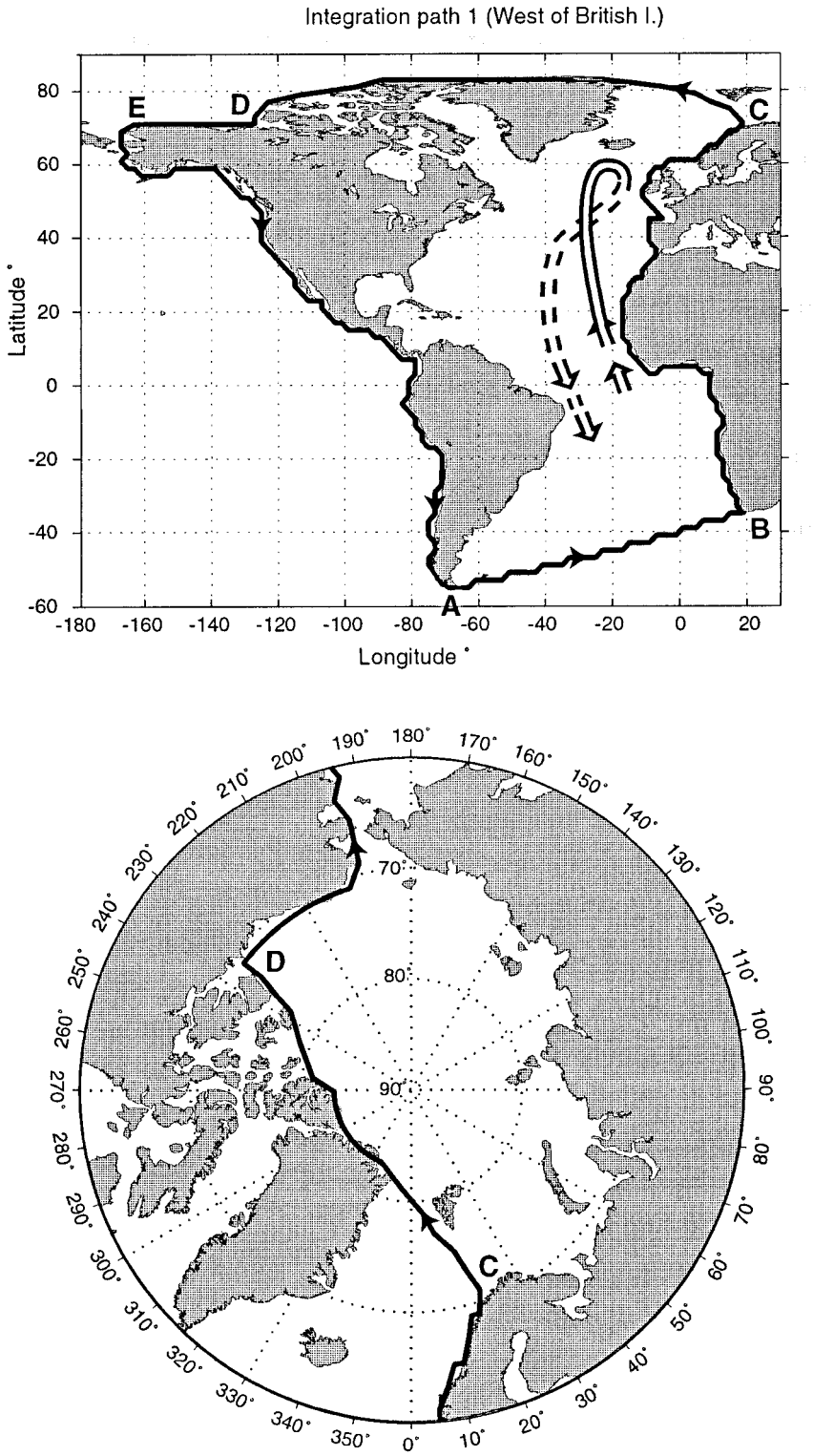

FIG. 3. A diagram of the closed integration path used in the realistic model (the second model). For clarity, a view of the path from a point above the north pole is also shown (bottom). Across the ocean the integration is done mainly in the zonal direction; along the eastern boundaries the coastline is followed. This model includes all NADW formations south of **CD**.

be important within the WBC. Namely, we assume that friction is neglected everywhere else including the eastern boundary currents. Our numerical simulation will later support this assumption.

Next, we define a vertically integrated pressure,

$$P^* = \int_{-\xi}^{\eta} P\, dz, \tag{2.5}$$

where ξ is the depth of the level of no horizontal pressure gradient (say, 1500 m) and η is the free surface vertical displacement. Using Leibniz's formula for the differentiation under the integral, one can show that

$$\frac{\partial P^*}{\partial x} = \int_{-\xi}^{\eta} \frac{\partial P}{\partial x}\, dz \quad \text{and} \quad \frac{\partial P^*}{\partial y} = \int_{-\xi}^{\eta} \frac{\partial P}{\partial y}\, dz \tag{2.6}$$

because $P = 0$ at $z = \eta, -\xi$. Using (2.6), vertical integration of (2.1)–(2.3) from $-\xi$ to η gives

$$-fV = -\frac{1}{\rho_0}\frac{\partial P^*}{\partial x} + \frac{\tau^x}{\rho} \tag{2.7}$$

$$fU = -\frac{1}{\rho_0}\frac{\partial P^*}{\partial y} - RV \tag{2.8}$$

$$\frac{\partial U}{\partial x} + \frac{\partial V}{\partial y} = 0, \tag{2.9}$$

where U and V are the vertically integrated transports in the x and y direction, and R is an interfacial friction coefficient, which, as we shall see, need not be specified for the purpose of our analysis. The equations are valid for all latitudes including the equator. Elimination of the pressure terms between (2.7) and (2.8) and consideration of (2.9) gives

$$\beta V = -\frac{1}{\rho}\frac{\partial \tau^x}{\partial y} - R\frac{\partial V}{\partial x}, \tag{2.10}$$

which, for the inviscid ocean interior, reduces to the familiar Sverdrup relationship

$$\beta V = -\frac{1}{\rho}\frac{\partial \tau^x}{\partial y}. \tag{2.11}$$

Five comments should be made with regard to (2.7)–(2.11):

1) Thermohaline effects enter the equations through the deviation of the hydrostatic pressure from the pressure associated with a state of rest.
2) Energy is supplied by both the wind and cooling; dissipation occurs through interfacial friction [i.e., the RV term in (2.8)] within the limits of the WBC system. Interfacial friction is not present in (2.7) because we assume that RU is small and negligible. Furthermore, since the velocities are small in the ocean interior the frictional term is taken to be negligible there.
3) Relation (2.7) holds both in the sluggish interior away from the boundaries and in the intense WBC where the flow is geostrophic in the cross-stream direction. Within the WBC the balance is between the Coriolis and pressure terms with the wind stress playing a secondary role. In the interior, on the other hand, the velocities are small and, consequently, all three terms are of the same order.
4) The inertial terms are excluded from the model but, to allow the interface to surface, nonlinearity is included in the pressure terms in the sense that the pressure deviations from a state of rest can be large. Since the model does not include relative vorticity within the WBC, it implicitly assumes that all the relative vorticity generated by moving the fluid meridionally (within the boundary layer) is dissipated immediately after its creation. This implies that cross-equatorial flows can easily take place via the WBC where the fluid does not ''remember'' its origin.
5) The frictional coefficient determines the width of the WBC but not its length (which, in turn, is controlled by the wind field and the pressure along the eastern boundary). In other words, the WBC adjusts its width in such a way that the total energy input (by the wind) is always dissipated along its base. Also, since in the interior the meridional transport is determined directly from the wind field (2.11), the total net meridional transport across the ocean is determined by the WBC.

b. Boundary conditions

The boundary condition along the solid boundaries is, of course, the familiar no-normal flow into the western and eastern walls. Since $U \equiv 0$ along the two eastern boundaries (**BD** and **A′C′**) it follows immediately from (2.8) with $RV \equiv 0$ that

$$P^* = \text{const along } \mathbf{BD} \text{ and } \mathbf{A'C'}. \tag{2.12}$$

As mentioned, along the western boundary the zonal velocity component also vanishes. However, in contrast to the eastern boundary, the pressure P^* is not uniform along this boundary due to the frictional term.

c. Integration of the momentum equation

To derive the transport formula for the first model, we integrate (2.7) from the western tips of the pseudo island to the eastern boundary (i.e., sections 1 and 2 shown in Fig. 1), noting that there is no transport through cross section **AB** because we require all the surface water that enters through **CD** to sink prior to reaching **AB**. We get

$$0 = -\frac{1}{\rho_0}(P^*_{\mathbf{B}} - P^*_{\mathbf{A}}) + \int_{\mathbf{A}}^{\mathbf{B}} \left(\frac{\tau^x}{\rho_0}\right) dx \tag{2.13a}$$

$$-f_2 T = -\frac{1}{\rho_0}(P^*_{\mathbf{D}} - P^*_{\mathbf{C}}) + \int_{\mathbf{C}}^{\mathbf{D}} \left(\frac{\tau^x}{\rho_0}\right) dx, \tag{2.13b}$$

where T is the net meridional transport across the ocean; f_2 is the Coriolis parameter along section 2; and the subscripts **A**, **B**, **C**, and **D** denote the location of the variable in question. In contrast to the classical closed basin approach that requires the WBC transport to be equal and opposite to the interior Sverdrup transport so that there is no net meridional transport (i.e., $T = 0$), we do not require the two transports to have any particular relationship. This implies that there can be a net meridional transport.

By subtracting (2.13b) from (2.13a) and taking into account the eastern boundary condition (2.12) we find the surprisingly simple relationship

$$T = -\frac{1}{f_2}\left[\int_{\mathbf{C}}^{\mathbf{D}} \frac{\tau^x}{\rho_0}\,dx + \int_{\mathbf{B}}^{\mathbf{A}} \frac{\tau^x}{\rho_0}\,dx\right]. \qquad (2.14)$$

This is our desired formula for the first simplified model that does not contain meridional winds. Note that, even though (2.14) looks like the familiar Ekman transport, it includes both the Ekman flow and the geostrophic flow underneath. Relation (2.14) gives the combined (wind and cooling) transport in terms of the wind field and the geography alone. This means that cooling controls the local dynamics (i.e., where and how the sinking occurs as well as the total amount of downwelling and upwelling) but does not directly control the net amount of water that enters the South Atlantic from the Southern Ocean. We shall return to this important point momentarily. Note that the main difference between (2.14) and the classical island rule formula derived by Godfrey (1989) is that (2.14) contains only the Coriolis parameter along the island's southern tip. Godfrey's formula includes the Coriolis parameters along both the southern and the northern tips because it does not involve any sinking. It is appropriate to point out, in passing, that Godfrey's original article gives the impression that he may not have recognized the fact that his derivation allows for fluid conversions within the moving layer.

3. Properties of the transport formula

In this section we shall describe several properties of (2.14) by answering questions that come immediately to mind. We shall also extend it to more general cases involving meridional winds and complex geography.

a. How does cooling enter the problem?

The expression for the meridional transport (2.14) does not contain any cooling *explicitly* because explicit cooling enters the problem only through the density that, with the Boussinesq approximation, does not affect the transport. However, the most important ways that cooling enters the problem are *implicit* rather than explicit.

First, cooling enters the problem implicitly through the location where the NADW is formed. To see this note that, if the region of NADW formation would have occurred north of **AB** (Fig. 1a), then the left-hand side of (2.13a) would have been $f_1 T$ (where f_1 is the Coriolis parameter at cross section 1) instead of zero. This gives

$$T = \oint \tau d/\rho_0 (f_1 - f_2),$$

which (since $f_1 \approx -f_2$) implies that the net meridional flow would be about half of what is given by (2.14). Hence, if the actual cooling is not sufficient to produce the transport given by (2.14), then the location of NADW formation would migrate northward so that the sinking would occur north of **AB**.

Second, cooling enters the problem implicitly through our assumption of no flow through the gap. Namely, if the cooling were reduced to a level below the rate corresponding to a formation region north of **AB** [i.e., half the rate given by (2.14)] or if it were eliminated altogether, then the water pushed by the wind into the Atlantic would have been going out of the Atlantic through the northern gap instead of as NADW. Since the actual gap is relatively small, hydraulic control would impose a limit on the amount that can go through it (probably a few Sverdrups; see, e.g., Pratt 1991). This might be accompanied by internal jumps and, consequently, neither (2.14) or (2.15) would apply.

b. What happens if there is no wind or a lot of wind?

According to (2.14), in the absence of wind there can be no net meridional flow into the Atlantic even if there is asymmetrical high-latitude cooling. This implies that without winds, whatever sinks in the North Atlantic must be compensated for by upwelling back into the upper layer somewhere else within the confines of the Atlantic.

Equation (2.14) also means that a state of no net meridional transport into the South Atlantic (i.e., a symmetrical problem) can change to a state with a net northward transport only if the problem becomes asymmetrical. This does not necessarily imply that the wind directly determines the amount of water sinking in the North Atlantic, but it does imply that sinking in general is accompanied by at least a partially compensating upwelling (elsewhere within the limits of the Atlantic). In this scenario the wind controls the *net* amount that is sinking.

In line with this logic, it is expected that increasing the winds along the tip of South America would decrease the amount of compensating upwelling (without directly affecting the sinking in the North Atlantic) and, hence, cause an *increase* in the net meridional transport. Similar results regarding the importance of southern winds were obtained numerically by Toggweiler and Samuels (1993, 1995).

c. The limits

The above properties can be summarized as follows:

1) In the limit of no cooling and moderate winds, the

wind would attempt to force all the water through the gap, hydraulic control and jumps would take place, and, as a result, our model would break down.
2) In the limit of very strong cooling and moderate winds, there will be more sinking than that given by (2.14) but there will also be more compensating upwelling (somewhere else in the Atlantic) with the final outcome of no change in the net conveyor transport.
3) In the limit of no wind ($\tau^x \equiv 0$), no water can get in and out of the Atlantic and whatever sinks in the North Atlantic has to upwell elsewhere within the Atlantic.
4) In the limit of very strong winds, some of the water will be forced beyond AB into the Pacific via the Bering Strait. In analogy with point (1) above, our model breaks down in this case.

d. Extension of the formula to a ''realistic'' model

It is a simple matter to extend the results of the first continuously stratified model to a more realistic model containing meridional winds and more complicated geometry (Fig. 3). As mentioned, we shall refer to this more realistic model as the second model. Using again the Boussinesq approximation and the vertically integrated equations in spherical coordinates, one ultimately arrives at the formula,

$$T = \oint \tau^l \, dl/(-f_0\rho_0), \tag{3.1}$$

where T is the total transport, f_0 the average Coriolis parameter along **AB** (Fig. 3), l indicates the component *along* the integration path, and, as before, the closed integration path contains the pseudo island. It is important to realize that (3.1) is no more than a counterclockwise integration of

$$-fV_n = -\frac{1}{\rho_0}\frac{\partial P^*}{\partial l} + \frac{\tau^l}{\rho_0},$$

(where V_n is the vertically integrated transport normal to the integration boundary l) along the closed contour. With such an integration the integral of the pressure gradient vanishes because we begin and end our integration at the same point.

Note that, as mentioned, (3.1) contains both zonal and meridional winds and that upwelling due to Ekman flows is, of course, a part of our vertically integrated transport. Recall that the only boundary condition that enters (3.1) is the no-flow condition along the eastern boundaries. By virtue of the generalized vertically integrated y momentum equation [analogous to (2.8)], this essentially implies that, along the eastern boundaries, the pressure gradient is balanced by the wind stress, that is, $\partial P^*/\partial l = \tau^l$. Using the Levitus data, this condition was verified by Godfrey (1989) for most of the world eastern boundaries. Masumoto and Yamagata (1993, 1996) also verified it (though indirectly) using general circulation models. Note that this condition (i.e., $\partial P^*/\partial l = \tau^l$) also holds along the northern cross section (section **CD**, Fig. 3) simply because there is no flow through it. Finally, it is important to realize that by taking the Coriolis parameter to be a constant along **AB** (Fig. 3) we introduced an error of 15%–30%.

e. Potential frictional effects

When interior frictional effects are not neglected, (3.1) takes the form

$$T = -\oint \frac{\tau^l}{f_0\partial_0}\, dl + \oint \frac{RV}{f_0}\, dl, \tag{3.2}$$

where V_s is the vertically integrated speed *tangential* to the integration boundary. It is difficult to come up with defensible values for the frictional coefficient R, but a value of 10^{-6} s^{-1} has been used before. It corresponds to a damping timescale of about 11 days, which is not unreasonable. Together with $V_s \sim 0.01$ m s^{-1} and $l \sim 20\,000$ km we get that the frictional forces can alter our estimate by approximately 2 Sv. A higher value of V_s (corresponding to, say, the Benguela or the Norwegian Current) may contribute a bit more (up to, say, a few Sverdrups) but not much more because these currents are relatively short ($\sim$1000 km). This neglected contribution is of the same order as other processes neglected in our calculation (e.g., the nonlinear self-propulsion of Agulhas rings, which is discussed later). Our numerical simulations that will be discussed later (section 4b) support this estimate.

4. Numerical simulations

Instead of verifying the above general transport formula (3.1) using very complicated numerical models (corresponding to Fig. 3), we examined numerically our first model, which does not contain meridional winds and very complicated geography. To examine the validity of the formula (2.14) we consider an application of a Bleck and Boudra ''reduced gravity'' isopycnic model to our first model. This numerical model has no thermodynamics, and to represent the overturning we introduce a (mass flux) source in the southeast corner and a sink in the northern Atlantic (north of the Gulf Stream). The mass flux associated with this source and sink is not a priori specified. Rather, we let the wind blow, measure the transport established across **CD** (Fig. 1a), and then require the source and sink to accommodate this measured transport. We continue to do so and continue to adjust the transport until a steady state is ultimately reached. Note that, since our formula gives the transport without giving the complete flow field, it is easiest to start the above runs from a state of rest. Consequently, the initial adjustments that we speak about are not small, but they do get smaller and smaller as we approach the predicted transport.

To verify that the computed transport is independent of the gap width, we first performed three sets of experiments where we varied only the gap width. As a second step, we varied the wind stress, measured the transport, and then plotted the theoretically computed transport versus the numerical transport. We shall see later that, because the southern winds are very strong, they contribute as much as 60% to the MOC transport. Consequently, we chose to vary the southern winds in our wind sensitivity experiments.

a. The numerical model

We used a reduced-gravity version of the isopycnic model developed by Bleck and Boudra (1981, 1986) and later improved by Bleck and Smith (1990). The advantage of this model is the use of the ''flux corrected transport'' algorithm (Boris and Book 1973; Zalesak 1979) for the solution of the continuity equation. This algorithm employs a higher-order correction to the depth calculations and allows the layers to outcrop and stay positive definite. The resulting scheme is virtually nondiffusive and conserves mass. For these reasons, the model is the most suitable model for our problem. The active layer is an enclosed feature, while the rest of the layer has zero depth. The modeled basin is a rectangle extending from 60°S to 60°N.

The equations of motion are the two momentum equations,

$$\frac{\partial u}{\partial t} + u\frac{\partial u}{\partial x} + v\frac{\partial u}{\partial y} - (f_0 + \beta y)v = -g'\frac{\partial h}{\partial x} + \frac{\nu}{h}\nabla\cdot(h\nabla u) + \frac{\tau_x}{\rho h} - Ku \quad (4.1)$$

$$\frac{\partial v}{\partial t} + u\frac{\partial v}{\partial x} + v\frac{\partial v}{\partial y} + (f_0 + \beta y)u = -g'\frac{\partial h}{\partial y} + \frac{\nu}{h}\nabla\cdot(h\nabla v) + \frac{\tau_y}{\rho h} - Kv, \quad (4.2)$$

and the continuity equation,

$$\frac{\partial h}{\partial t} + \frac{\partial (hu)}{\partial x} + \frac{\partial (hv)}{\partial y} = 0, \quad (4.3)$$

where, as before, the notation is conventional.

The model uses the Arakawa (1966) C-grid. The u velocity points are shifted one-half grid step to the left from the h points, the v velocity points are shifted one-half grid step down from the h points, and the vorticity points are shifted one-half grid step down from the u velocity points. This grid allows for reducing the order of errors in the numerical scheme. The solution is advanced in time using the leapfrog scheme. The velocity fields are smoothed in time in order to stabilize the numerical procedure. The velocities for the weightless grid points are set to zero.

To make our runs more economical, we artificially magnified both β and the wind stress and artificially reduced both the meridional and zonal basin scales (see Table 1 and Figs. 4a,b). The linear drag coefficient, K, was also increased so that the increased wind stress is balanced. With these modifications we had a dramatic reduction in the grid count and, consequently, our runs lasted for about 40 minutes (each) instead of a week or so that each run would have lasted had we not modified β, the wind stress, and the basin size.

The downside of the above modifications is an unnaturally large ratio between eddy size (the Rossby radius) and basin size. As we shall shortly see, this is not really a difficulty in our runs because in our case the eddies do not play a major role in the meridional mass exchange. Furthermore, this unnatural eddy–basin ratio issue can be easily resolved by using a very large horizontal eddy viscosity coefficient that eliminates any long-lived eddies such as Gulf Stream rings. This essentially implies that our model is not an eddy-resolving model. Note also that, with our chosen parameters, the ratio between the Munk layer thickness $(\nu/\beta)^{1/3}$ and the basin size was still very small (as required) because our β is magnified.

Before presenting our results it is useful to recall that the main difference between our calculation and the original island calculation of Godfrey (1989) [which has been later verified numerically by many others (e.g., Masumoto and Yamagata 1993, 1996)] is the absence of flow through the northern gap. In view of this, it is instructive to examine how sensitive the results are to the width of the northern gap and the flow through it. In other words, it is useful to know how narrow can the gap be and still be regarded as an ''equalizer'' of the pressure field on the two sides. For this reason, we performed three sets of experiments (A, B, and C) where we varied both the northern gap width and the resolution. We then proceeded and performed a set of experiments that examined the sensitivity of our results to the wind field (set D). The simplified wind stress profile that we used (adopted from Hellerman and Rosenstein 1983) is shown in Fig. 4a.

b. Results

Our results are shown in Figs. 5, 6, 7, and 8. Experiments 35–40 (set D) correspond to a transport comparable to that of the actual MOC (10–15 Sv). Figures 5, 6, and 7 show the observed (numerical) transports and their relationship to the analytics. We see that, even though our eddy viscosity is large (16 000 $m^2\ s^{-1}$), there is an exceptionally good agreement between the nonlinear numerical simulations and the quasi-linear analytical computation no matter how narrow the gap is or how strong the wind is. This remarkable agreement shows that full nonlinearity, linear drag, and lateral friction (included in the numerics but absent from the analytics) are all unimportant. Furthermore, it shows that, as expected, the large eddy viscosity is compensated by

TABLE 1. A description of the three variable gap width sets (A, B, and C) of numerical experiments (employing a one-and-a half-layer version of the Bleck and Boudra model). The variable wind experiments (set D, experiments 25–45) are not listed in the table as their only variable is the wind profile shown in Fig. 4a. In all experiments $g' = 0.015$ m s^{-7} and H = 600 m.

Set	Description	Expt	Δx Δy Δt	β (10^{-11} m^{-1} s^{-1})	υ (m^2 s^{-1})	Wind stress magnification factor	Munk layer thickness (km)	K (10^{-6} s^{-1})	R_d (km)	Shown in fig.	Number of grid points in gap
A	Large basin (2640 × 600 km), low resolution see Fig. 4b)	1	15 km	11.5	16,000		52	2	28	5	26
		2	15 km								21
		3	360 s								16
		4									11
		5									gap closed
B	Large basin (2640 × 600 km), high resolution (see Fig. 4b)	6	15 km	11.5	16,000		52	2	28	5	6
		7	5 km								4
		8	120 s								2
		9									1
C	Small basin (176 × 40 km), high resolution (see Fig. 4b)	10	1 km	172.5		15	10	25	28	6	26
		11	1 km								24
		12	24 s								22
		13									20
		14									18
		15									16
		16									14
		17									12
		18									10
		19									8
		20									6
		21						}			4
		22						} 25			3
		23						}			2
		24						25			irrelevant (gap closed)

our magnified β and magnified wind stress. Experiments 5 and 24 correspond to closed gaps so that our analytical formula does not apply.

Figures 5 and 6 show that the results are independent of the gap's width. Even for gaps as narrow as $0.05R_d$, our analytical results are in excellent agreement with the numerics. This is due to the fact that the gap's role is merely to equalize the pressure across it; it is not necessary that any water will flow through it. Figure 7 shows that, as the wind stress is increased linearly along **CD**, both the analytical and the numerical transports increase linearly. However, the analytical transport increases at a rate 78% of the numerical growth rate. Since our analytical formula does not involve a detailed solution of the entire flow field, it is very difficult to determine why this is so.

One might be tempted to attribute the difference between the two estimates to the linear drag along the eastern boundaries, which, though small, is the largest neglected term at least for some of the experiments (see Fig. 8). However, since this drag always opposes the throughflow (in the sense that it requires the theoretical transport to be always larger than the numerical), it cannot be the agent responsible for the discrepancy displayed in Fig. 7. Figure 8 shows the relative importance of the various terms in the integrated momentum equation. We see that, as is assumed in the analytics, lateral friction, linear drag, and advection are all small and negligible.

Typical thickness and transport contours corresponding to simulations with broad and very narrow gaps are shown in Figs. 9 and 10. Figures 9 and 10 also show how the MOC (shaded) crosses the equator. It begins along the eastern boundary of the South Atlantic and proceeds westward as a south equatorial current. As earlier studies predicted (see, e.g., Killworth 1991) it then crosses the equator as a WBC. It finally reaches the central basin after progressing along the northern edge of the gyre. Also, note that the thickness contours shown in Figs. 9 and 10 clearly support our boundary conditions. Since there are no meridional winds in this first model, the eastern boundary condition is that the pressure is constant along the eastern boundaries. The thickness contours along both the eastern boundary of the eastern basin and the western side of the island show very clearly that this is indeed the case. Furthermore, note that along the solid zonal boundaries (to be distinguished from our zonal integration path), the pressure gradient is proportional to the zonal wind stress as there is no flow into these boundaries.

Before proceeding and discussing the application of our formula, it is appropriate to point out that an interesting extension of our numerical experiments would be to introduce additional sources and sinks and see

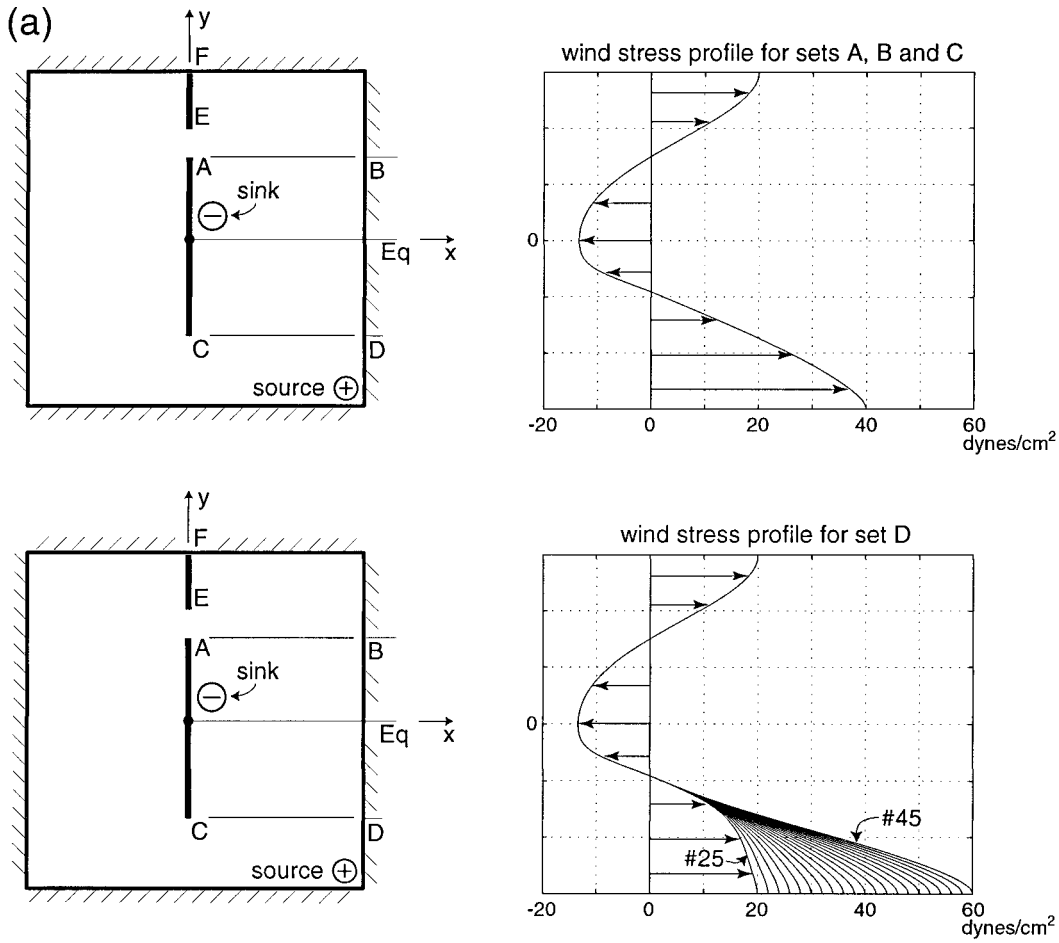

FIG. 4a. Schematics of the (1½ layer) source–sink numerical experiments and the magnified (and simplified) zonal wind stress as a function of latitude (adapted from Hellerman and Rosenstein 1983). The model has no thermohaline processes in it; instead, the mass flux exiting the source ⊕ and entering the sink ⊖ represents the conveyor upper limb. It was not specified a priori. Rather, we let the wind blow for a while, measured the transport across **CD**, and then required the sink and source to accommodate the measured amount (going through **CD**). The procedure was then repeated continuously and the source mass flux was continuously adjusted until a steady state was reached. As shown, the original experiments have the sink in the middle of the basin (corresponding to the Labrador and Norwegian Seas). However, to expedite the time required for the model to reach a steady state, most of the experiments were performed with the sink situated in the western part of the Atlantic basin (see Fig. 4b). The top right panel shows the (fixed) wind profile used for the variable gap width experiments (sets A, B, and C), whereas the bottom right panel shows the variable wind profile that we used (set D).

how the flow field is altered. In particular, it would be of interest to take the steady-state experiments, add sources and sinks, and see whether the additional mass flux reaches the (added) sink via the Atlantic or the Pacific basin. It would be necessary to conduct a family of such experiments in order to reach meaningful conclusions, as the solutions would depend on the location of the sources and sinks. One's initial (and erroneous) guess is that the results of these experiments can be easily predicted in advance because the problem is linear so that the solutions can simply be added up. Although the solutions can indeed be added up, the analysis is not at all trivial as even the source–sink flows by themselves cannot be easily determined in advance.

5. The interhemispheric transport in the Atlantic

We used NCEP reanalysis data[1] for annual mean winds (averaged over 40 years) with a drag coefficient of 1.6×10^{-3} [which is the appropriate coefficient for winds (such as ours) with a speed of less than 6.7 m s^{-1} (see, e.g., Hellerman and Rosenstein 1983)]. Along the chosen path (Fig. 3), the integration was done over $2° \times 2°$ boxes. With the aid of (3.1) one finds a rea-

[1] Provided by the NOAA–CIRES Climate Diagnostics Center, Boulder, Colorado, from their Web site at http://www.cdc.noaa.gov.

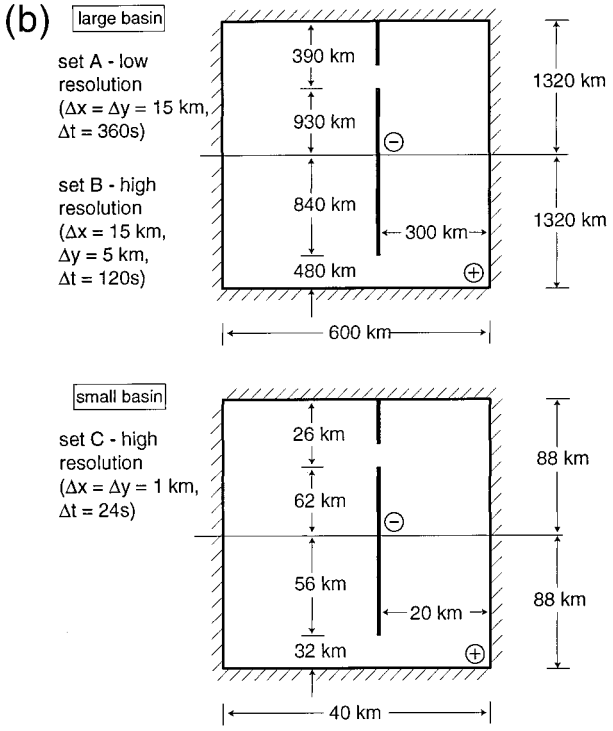

FIG. 4b. The dimensions of the basins used for the varying gap width experiments (sets A, B, and C).

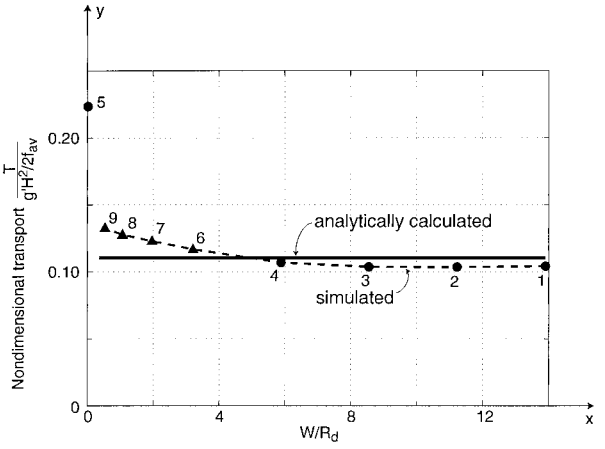

FIG. 5. A comparison of the analytically calculated meridional transport for the first model (solid line) and the numerically simulated values (dashed line). (Numerals indicate experiment number.) Solid dots indicate simulations with a 5×15 km resolution (set A), whereas solid triangles indicate simulations with higher resolution of 5×15 km (set B). With the high-resolution experiments there were at least three grid points across the gap even when the gap was half the Rossby radius. In all shown experiments the sink was situated next to the western boundary (and north of the equator). Experiment 5 corresponds to a closed gap. Note that the agreement between the analytics and the numerics is excellent. Physical constants: $g' = 0.015$ m s^{-2}; $H = 600$ m; $\beta = 172.5 \times 10^{-11}$ m^{-1} s^{-1}; $\nu = 1.6 \times 10^{4}$ m^2 s^{-1}; $K = 2 \times 10^{-6}$ s^{-1}; $R_d = 28$ km; $f_{\max} = 1.52 \times 10^{-4}$ s^{-1} (where $f_{\max}$ is the Coriolis parameter at the northern tip of the island). Transport was nondimensionalized with $g'H^2/2f_{\text{av}}$ (where f_{av} is the average Coriolis parameter, 0.76×10^{-4} s^{-1}).

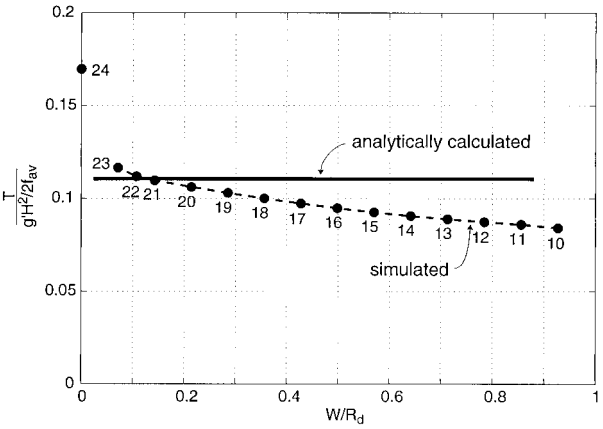

FIG. 6. As in Fig. 5 except that we show here the results of the very high resolution experiments (set C). For a comparison, we also show the result of expt 24 that corresponds to a completely closed gap (not captured by our theory). In the experiments shown here, we closed the gap almost completely (the smallest width corresponded to $W/R_d < 0.1$) and still maintained at least three grid points across it.

sonable net meridional transport of about 9 Sv; 60% of this transport is due to the (strong) southern winds.

Before proceeding and discussing the implication of this calculation, it is appropriate to discuss the role that Agulhas rings play in the problem and the limitations of our analysis.

a. Agulhas rings

Both observations and wind-driven circulation models show that there is a transfer of Indian Ocean thermocline water into the South Atlantic (Boudra and Chassignet 1988; Semtner and Chervin 1988; Gordon and Haxby 1990). Most of the leakage is achieved via

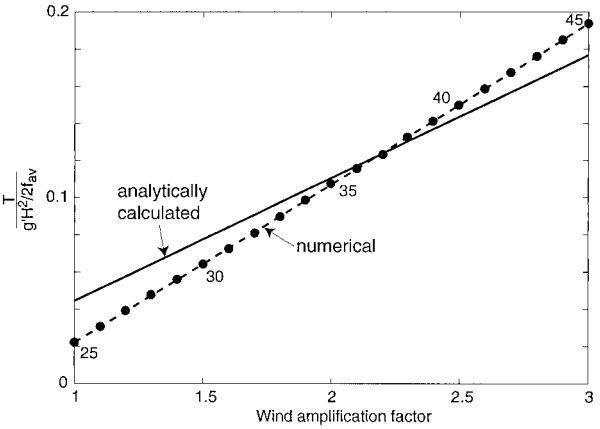

FIG. 7. As in Fig. 5 except that we show here the results of the numerical simulations with the varying wind pattern (set D) shown in the lower panel of Fig. 4a. As before, numerals indicate the experiment number. Expts 35–40 correspond to a nondimensional transport comparable to that of the actual MOC (10–15 Sv). Note that the agreement is excellent in most cases. The agreement is not so good, however, when the transport is very small (1–2 Sv).

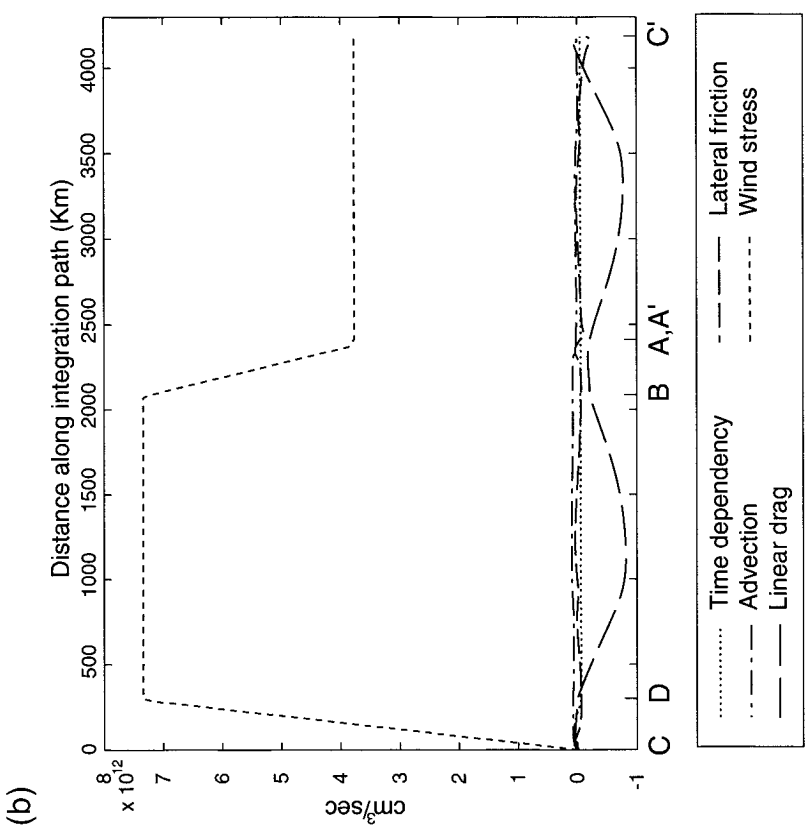

FIG. 8a. A comparison of the various terms in the momentum equation (used to derive the analytical formula) along the integration path (CDBAA'C', Fig. 1a). Here we show expt 4 (all experiments show very similar results). Note that all the terms that have been assumed to be small in the analytical derivation are indeed small, i.e., time dependency, advection, linear drag, and lateral friction. All fall practically on the zero line. The dominant terms are Coriolis, pressure gradient, and the wind stress, all of which are included in the analytical derivation.

FIG. 8b. The line integrals of the neglected terms shown in (a) and the line integral of the wind stress. Note that the neglected integrated advection, lateral fiction, and time dependency are almost zero as should be the case. The largest (integrated) neglected term is the (accumulated) linear drag that at some locations can reach as much as 20% of the (accumulated) wind stress. Note that this term actually integrates to almost zero over our contour due to the partial symmetry of the wind field over the two hemispheres.

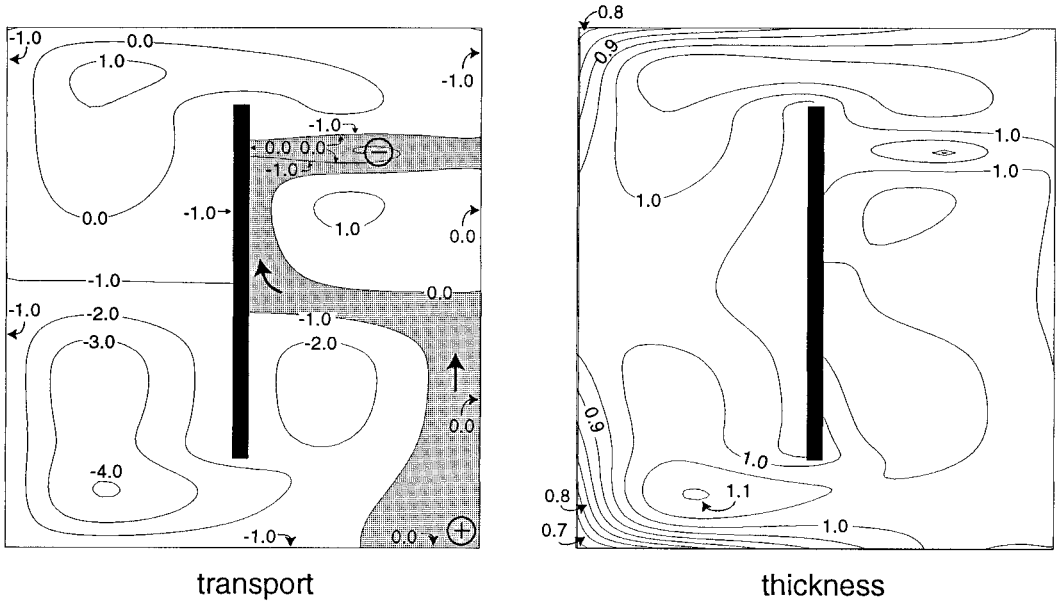

FIG. 9. Nondimensional transport and thickness contours for a typical numerical simulation with a broad northern gap. Here, the sink is situated in the middle of the ocean and, consequently, there is a discontinuity in the transport function along both the island and the eastern boundary. (The experiments listed in Table 1 and shown in Figs. 5, 6, and 7 were conducted with the sink immediately to the east of the island because they reached a steady state considerably faster than the one shown here with the sink in the center of the basin. This is due to the tendency of the upper fluid to surface in the vicinity of the open ocean sink.) To assure that the transport is nondimensionalized with increments equal to the source–sink mass flux, dimensional values were divided by $0.12(g'H^2/2f_{av})$. Thickness contours were nondimensionalized with 300 m. Note that, along both the eastern boundary of the eastern basin and the eastern boundary of the western basin (i.e., the western boundary of the island), the thickness does not vary with y because, in this simple case, there are no meridional winds. This is in agreement with the analytics. Also, note that along the solid zonal boundaries (to be distinguished from our zonal integration boundaries which go through the tips of the island) the pressure gradient balances the wind stress ($\partial P^*/\partial l = \tau^l$) because there is no meridional flow through these boundaries.

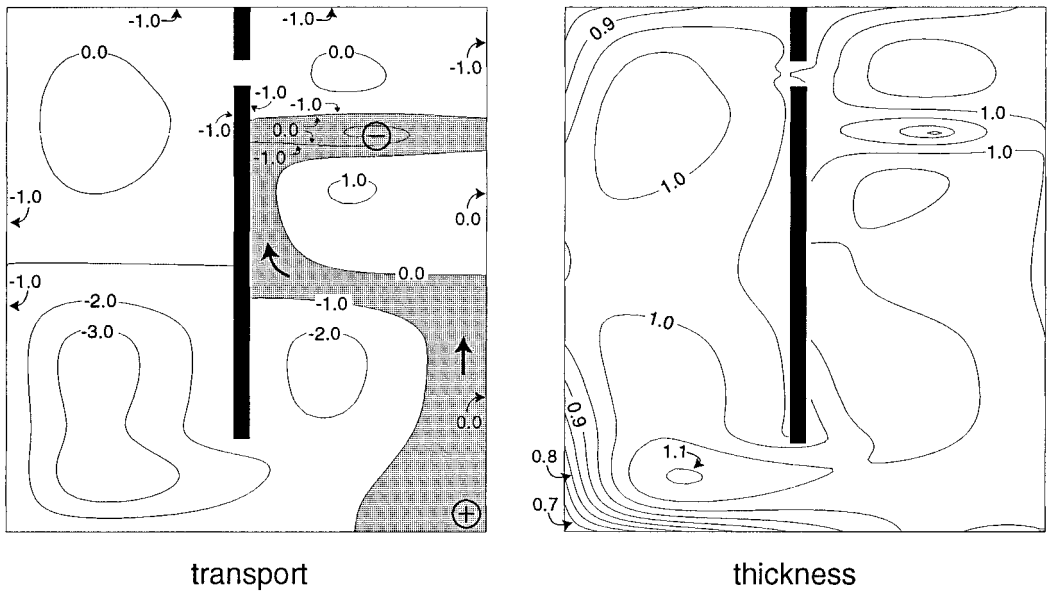

FIG. 10. As in Fig. 9 except that we show here the results for a very narrow gap. Transport contours were nondimensionalized with $0.13(g'H^2/2f_{av})$ and thickness contours with 300 m. Note that the fact that the gap is very narrow has virtually no bearing on the MOC transport.

Agulhas rings (Olson and Evans 1986; Lutjeharms and Gordon 1987; Lutjeharms and van Ballegooyen 1988), but additional Indian Ocean waters are injected into the Atlantic via plumes (Olson and Evans 1986; Lutjeharms 1988; Lutjeharms and Valentine 1988). Also, surface waters are sometimes entrained by the Benguela Current (Nelson and Hutchings 1983; Shannon 1985). Estimates of the above leakage vary considerably due to various measuring techniques and (perhaps) due to actual variability.

Gordon et al. (1987) arrived at an estimate of 10 Sv for water entering the Atlantic in 1983, whereas Whitworth and Nowlin (1987) observed a much larger transport of 20 Sv in 1984. Bennett (1988), on the other hand, arrived at lower values of 6.3 and 9.6 Sv for 1983 and 1984. From these amounts that enter the Atlantic, Bennett argues that only 2.8 Sv are warm Indian Ocean water. Stramma and Peterson (1990) find an Indian to Atlantic transfer of 8 Sv, whereas Gordon and Haxby's (1990) inventory of rings suggest a transport of 10–15 Sv. The McCartney and Woodgate-Jones (1991) definition of an eddy corresponds to a smaller feature than that considered by Gordon and Haxby (1990), and consequently, they arrive at a smaller estimate of 2–5 Sv. Byrne et al. (1995) estimated the flux to be at least 5 Sv; the most recent and most extensive estimate is that of Goñi et al. (1997), who arrive at an average influx of no more than 4–5 Sv. Since it is the most updated estimate we shall use this latter value as a typical mass flux of warm Indian Ocean water into the South Atlantic [even though it is somewhat smaller than previous values (see also van Ballegooyen et al. 1994; Duncombe Rae et al. 1996)].

Olson and Evans (1986) estimate that the rings translate toward the northwest at a rate of 5–8 cm s^{-1}. Goñi et al. (1997) arrive at a similar rate of 5–14 cm s^{-1}. A fourth of this speed is probably due to the familiar β-induced speed that, for rings with a diameter of 400–500 km, a depth of 800 m, and a reduced gravity of 2×10^{-2} m s^{-2}, is no more than 1.5 cm s^{-1}. [This can be easily verified by recalling that such rings translate at a speed smaller than $0.4\beta R_d^2$, where R_d is the Rossby radius based on the ring's maximum depth (see, e.g., Nof 1981).] Another fourth of the observed migration speed is due to advection by the local Sverdrup flow (see Fig. 6) and the remaining half (3–7 cm s^{-1}) cannot be clearly accounted for. {It can possibly be due to bottom topography that increases the migration rate [see, e.g., Dewar and Gailliard (1994) but also Kamenkovich et al. (1996) where a counterexample of a reduced rate is given] or due to a dipolar structure (Radko 1997).} Regardless of the causes for this unaccounted speed, we can conclude that out of the 4–5 Sv influx, about 1.5 Sv is due to advection by the surrounding flow that obeys Sverdrup dynamics and, hence, is *included* in our calculations. Namely, in our calculations, 3–4 Sv, at the most, are neglected because of the absence of the ring self-propulsion mechanism. Although definitely not entirely negligible, this is a relatively small amount compared to the observed 10 Sv or so of the interhemispheric flow.

b. Limitations

Two aspects of the model could perhaps be problematic. The first is the Gulf of Guinea where the boundary of the continent is approximately zonal so that a strong boundary current (not captured by our eastern boundary condition) can perhaps develop. Examination of the offshore Sverdrup transports (which can produce the boundary current in question) as well as Hisard et al.'s (1986) measurements (conducted during 1984, an admittedly anomalous year) reveal, however, that an average 10 Sv transport in the Gulf of Guinea is highly unlikely. This is consistent with Godfrey's verification of the boundary condition $\partial P^*/\partial l = \tau^l$ along the eastern boundaries of the world ocean. The possibility of introducing severe errors with our treatment of the Gulf of Guinea is, therefore, rejected. The second possibility is that nonlinear eddy-driven flows in the southeastern Atlantic (neglected in both the analytics and numerics) transfer the excess amount of water necessary for the conveyor closure. Recent measurements of the Benguela Current (Peterson and Stramma 1991; Clement and Gordon 1995; Garzoli et al. 1996, 1997) suggest, however, that there is a difference of merely a few Sverdrups between the calculated Sverdrup transport (included in both the analytical and the numerical models) and the measured Benguela Current transport. Overall, we can say that all eastern nonlinear processes (e.g., Agulhas rings, the Benguela Current, the Norwegian Current) may affect our estimation (of 9 Sv) by a few Sverdrups.

6. Summary and discussion

To circumvent solving the (incredibly complicated) wind–thermohaline problem we have adopted an analytical technique where the Americas are taken to be a pseudo island and the linearized equations of motion are integrated around a region containing both the island and the ocean to its east and north. We have considered two models. The first is a rectangular model subject to thermohaline processes and zonal winds (Figs. 1 and 2). The second is a more ''realistic'' model subject to thermohaline as well as zonal and meridional winds (Fig. 3). In both models the interior is governed by Sverdrup dynamics and the WBC is dissipative in nature. Surface cooling and heating that are not severe enough to produce NADW are allowed everywhere and need not be specified. Severe cooling (i.e., cooling that is strong enough to produce NADW) need not be explicitly specified either. However, such severe cooling enters both models implicitly through the location of the NADW formation that needs to be, in general, specified. (In our second, realistic model we specified this severe cooling to take place south of cross section **CD**

shown in Fig. 3, implying that there is no flow via the Bering Strait.) Our analytical model includes some nonlinearity (through the pressure terms) but the inertial terms are neglected and the motions are primarily geostrophic.

Both models are open on the southern side (so that a free exchange with the Southern Ocean is allowed) and partially open on the northwest side. This partial connection allows for a minimal flow through the Bering Strait, assuring the continuation of pressure around the Americas. A net northward interhemispheric flow of upper water ($\sigma_\theta < 27.80$) is permitted; that is, the WBC transport is not necessarily equal and opposite to the integrated interior transport (Figs. 1, 2, and 3). This net northward transport is cooled by the atmosphere at high latitudes; it sinks and returns southward as the NADW. An inert layer is sandwiched between the northward flowing upper water ($\sigma_\theta < 27.80$) and the southward flowing NADW ($\sigma_\theta > 27.80$).

Our analytical solution for both models enables one to obtain the net northward transport (of thermohaline and intermediate water) directly from the wind field and the geography. The derivation of the analytical solution is based on the fact that the integral of the (long path) pressure gradient $\partial P^*/\partial l$ along a closed contour (l) is zero. (This does not necessarily mean that the pressure is a constant along the boundary but rather that, if the pressure goes up somewhere, it must also go down somewhere else along the contour so that, ultimately, it comes back to the origination point with a magnitude identical to the initial value.) The solution shows that there must be a latitudinal variation in the wind field (or the shape of the continents) in order for such a meridional transport of water to exist. The analytical results for the first (rectangular model) were compared in detail to numerical simulations using an isopycnic model (without thermodynamics) and an excellent agreement was in general found (Figs. 5, 6, 7, and 8). The comparison shows that the results are not very sensitive to the problem parameters (i.e., the width of the northern gap or the presence of some small flow through it) and that the neglected terms are indeed small. It is worth pointing out here that, since the theoretical problem is linear, the solutions are additives so that any solution can be superimposed on a known solution.

The calculation of the transport associated with the second model was obtained by integrating the momentum equations using 40 years of NCEP data. The transport derived in this fashion contains some of the Agulhas ring mass flux, save the self-propelled transport. We found that the calculated MOC transport is about 9 Sv. All the high-latitudinal coastlines were taken to be ice free but including ice and assuming no wind stress transfer across it makes practically no difference in our results as 60% of the transport is driven by the (strong) southern winds. It is estimated that the Benguela Current, Agulhas rings, and other nonlinear processes may add several more Sverdrups to the above transport. AABW entering the South Atlantic from the Southern Ocean (several Sverdrups) is not included in the above estimate.

In summary, it is suggested (on the basis of the excellent agreement between the analytics and the numerics) that the transport of the MOC can be estimated from the wind field, the observed position of the NADW formation, and the observation that, although the Bering Strait allows the pressure across it to be continuous, there is no significant flow through it. The main error in our calculation is due to the linearization of the ocean interior, which involves the neglect of the nonlinear self-propulsion of Agulhas rings and the nonlinearity of eastern boundary currents. All of these processes can probably affect our results by a few (or several) Sverdrups.

Finally, it should be stressed that, although the agreement between the analytics and the numerics is informative, the numerical simulations do not completely validate our analytical results as, in order do so, it is necessary to use a model with thermodynamics. Specifically, it is necessary to conduct experiments with variable diabatic forcing and constant wind and show that the MOC transport remains constant. It is hoped that these aspects will be examined with more detail in the future using both more general numerical simulations and observations.

Acknowledgments. This study was supported by the National Science Foundation under Contracts OCE 9503816 and 9633655; National Aeronautics and Space Administration Grants NAGW-4883, NAG5-7630, NSG5-7630, and NGT5-30164; and Office of Naval Research Grant N00014-89-J-1606. Discussions with G. Weatherly were very useful. Computations were done by S. Van Gorder and drawings by Beth Raynor.

APPENDIX

List of Symbols

f_0	Coriolis parameter along **AB** (Fig. 3)
f_1	Coriolis parameter along section 1 (Fig. 1a)
f_2	Coriolis parameter along section 2 (Fig. 1a)
F_{av}	Average Coriolis parameter, 0.76×10^{-1} s^{-1}
F_{max}	Coriolis parameter at the northern tip of the island
g'	Reduced gravity, $(\Delta\rho/\rho)g$
K	Linear drag coefficient
k	Diffusion coefficient
l	Integration path
P	Deviation of the hydrostatic pressure from the pressure associated with a state of rest
P^*	Vertically integrated pressure
R	Interfacial friction coefficient
T	Net meridional transport across the ocean
U, V	Vertically integrated transports in the x and y directions
u, v, w	Velocities in the x, y, and z directions

η	Free surface vertical displacement
ν	Viscosity
ρ_0	Uniform density of the motionless deep water
ρ'	Density deviation
τ^l	Wind stress along the integration path (l)
τ^x	Wind stress in the x direction
τ^y	Stress in the y direction
ξ	Depth of the level of no horizontal pressure gradient (measured positively upward)

REFERENCES

Arakawa, A., 1966: Computational design for long-term numerical integration of the equations of fluid motion. Two-dimensional incompressible flow. Part I. *J. Comput. Phys.,* **1,** 119–143.

Barnier, B., P. Marchesiello, A. P. de Miranda, J.-M. Molines, and M. Coulibaly, 1998: A sigma-coordinate primitive equation model for studying the circulation in the South Atlantic. Part I: Model configuration with error estimates. *Deep-Sea Res. I,* **45,** 543–572.

Bennett, S. L., 1988: Where three oceans meet: The Agulhas retroflection region. Ph.D. thesis, MIT/WHOI Rep. WHOI-88-51, xxvii + 367 pp. [Available from MBL-WHOI Library, Woods Hole, MA 02543.]

Bleck, R., and D. Boudra, 1981: Initial testing of a numerical ocean circulation model using a hybrid (quasi-isopycnic) vertical coordinate. *J. Phys. Oceanogr.,* **11,** 755–770.

——, and ——, 1986: Wind-driven spin-up in eddy-resolving ocean models formulated in isopycnic and isobaric coordinates. *J. Geophys. Res.,* **91,** 7611–7621.

——, and L. Smith, 1990: A wind-driven isopycnic coordinate model of the north and equatorial Atlantic Ocean. 1. Model development and supporting experiments. *J. Geophys. Res.,* **95,** 3273–3285.

Boris, J., and D. Book, 1973: Flux-corrected transport. I. SHASTA, A fluid transport algorithm that works. *J. Comput. Phys.,* **11,** 38–69.

Boudra, D. B., and E. P. Chassignet, 1988: Dynamics of Agulhas retroflection and ring formation in a numerical model. Part I: The vorticity balance. *J. Phys. Oceanogr.,* **18,** 280–303.

Byrne, D. A., A. L. Gordon, and W. F. Haxby, 1995: Agulhas eddies: A synoptic view using Geosat ERM data. *J. Phys. Oceanogr.,* **25,** 902–917.

Clement, A. C., and A. L. Gordon, 1995: The absolute velocity field of Agulhas eddies and the Benguela Current. *J. Geophys. Res.,* **100,** 22 591–22 601.

Dewar, W. K., and C. Gailliard, 1994: The dynamics of barotropically dominated rings. *J. Phys. Oceanogr.,* **24,** 5–29.

Drijfhout, S. S., E. Maier-Reimer, and U. Mikolajewicz, 1996: Tracing the conveyor belt in the Hamburg large-scale geostrophic ocean general circulation model. *J. Geophys. Res.,* **101,** 22 563–22 575.

Duncombe Rae, C. M., S. L. Garzoli, and A. L. Gordon, 1996: The eddy field of the southeast Atlantic Ocean: A statistical census from the BEST project. *J. Geophys. Res.,* **101,** 11 949–11 964.

Garzoli, S. L., A. L. Gordon, V. Kamenkovich, D. Pillsbury, and C. Duncombe-Rae, 1996: Variability and sources of the southeastern Atlantic circulation. *J. Mar. Res.,* **54,** 1039–1071.

——, G. J. Goñi, A. J. Mariano, and D. B. Olson, 1997: Monitoring the upper southeastern Atlantic transports using altimeter data. *J. Mar. Res.,* **55,** 453–481.

Godfrey, J. S., 1989: A Sverdrup model of the depth-integrated flow for the world ocean allowing for island circulations. *Geophys. Astrophys. Fluid Dyn.,* **45,** 89–112.

Goñi, G., S. Garzoli, A. Roubicek, D. Olson, and O. Brown, 1997: Agulhas ring dynamics from TOPEX/POSEIDON satellite altimeter data. *J. Mar. Res.,* **55,** 861–883.

Gordon, A. L., 1986: Inter-ocean exchange of thermocline water. *J. Geophys. Res.,* **91,** 5037–5050.

——, and W. F. Haxby, 1990: Agulhas eddies invade the South Atlantic: Evidence from geosat altimeter and shipboard conductivity–temperature–depth survey. *J. Geophys. Res.,* **95,** 3117–3127.

——, J. R. E. Lutjeharms, and M. L. Gründlingh, 1987: Stratification and circulaton at the Agulhas retroflection. *Deep-Sea Res.,* **34,** 565–599.

——, W. F. Ray, W. M. Smethie, and M. J. Warner, 1992: Thermocline and intermediate water communication between the South Atlantic and the Indian Oceans. *J. Geophys. Res.,* **97,** 7223–7240.

Hellerman, S., and M. Rosenstein, 1983: Normal monthly wind stress over the world ocean with error estimates. *J. Phys. Oceanogr.,* **13,** 1093–1104.

Hisard, P., C. Henin, R. Goughton, B. Piton, and P. Rual, 1986: Oceanic conditions in the tropical Atlantic during 1983 and 1984. *Nature,* **322,** 243–245.

Kamenkovich, V. M., Y. P. Leonov, D. A. Nechaev, D. A. Byrne, and A. L. Gordon, 1996: On the influence of bottom topography on the Agulhas eddy. *J. Phys. Oceanogr.,* **26,** 892–912.

Killworth, P. D., 1991: Cross-equatorial geostrophic adjustment. *J. Phys. Oceanogr.,* **21,** 1581–1601.

Lutjeharms, J. R. E., 1988: Examples of extreme circulation events at the Agulhas retroflection. *S. Afr. J. Sci.,* **84,** 584–586.

——, and A. L. Gordon, 1987: Shedding of an Agulhas ring observed at sea. *Nature,* **325,** 138–140.

——, and H. R. Valentine, 1988: Eddies at the subtropical convergence south of Africa. *J. Phys. Oceanogr.,* **18,** 761–774.

——, and R. C. van Ballegooyen, 1988: Anomalous upstream retroflection in the Agulhas Current. *Science,* **240,** 1770–1772.

Marchesiello, P., B. Barnier, and A. P. de Miranda, 1998: A sigma-coordinate primitive equation model for studying the circulation in the South Atlantic. Part II: Meridional transports and seasonal variability. *Deep-Sea Res.,* **45,** 573–608.

Masumoto, Y., and T. Yamagata, 1993: Simulated seasonal circulation in the Indonesian Seas. *J. Geophys. Res.,* **98,** 12 501–12 509.

——, and ——, 1996: Seasonal variations of the Indonesian throughflow in a general ocean circulation model. *J. Geophys. Res.,* **101,** 12 287–12 294.

Matano, R. P., and S. G. H. Philander, 1993: Heat and mass balances of the South Atlantic Ocean calculated from a numerical model. *J. Geophys. Res.,* **98,** 977–984.

McCartney, M. S., and M. E. Woodgate-Jones, 1991: A deep-reaching anticyclonic eddy in the subtropical gyre of the eastern South Atlantic. *Deep-Sea Res.,* **38,** S411–S443.

Nelson, G., and L. Hutchings, 1983: The Benguela upwelling area. *Progress in Oceanography,* Vol. 12, Pergamon, 333–356.

Nof, D., 1981: On the β-induced movement of isolated baroclinic eddies. *J. Phys. Oceanogr.,* **11,** 1662–1672.

——, and S. Van Gorder, 1999: A different perspective on the export of water from the South Atlantic. *J. Phys. Oceanogr.,* **29,** 2285–2302.

Olson, D. B., and R. H. Evans, 1986: Rings of the Agulhas Current. *Deep-Sea Res.,* **33,** 27–42.

Parsons, A. T., 1969: A two-layer model of Gulf Stream separation. *J. Fluid. Mech.,* **39,** 511–528.

Pedlosky, J., L. J. Pratt, M. A. Spall, and K. R. Helfrich, 1997: Circulation around islands and ridges. *J. Mar. Res.,* **55,** 1199–1251.

Peterson, R. G., and L. Stramma, 1991: Upper-level circulation in the South Atlantic Ocean. *Progress in Oceanography,* Vol. 26, Pergamon, 1–73.

Pratt, L., 1991: Geostrophic versus critical control in straits. *J. Phys. Oceanogr.,* **21,** 728–732.

——, and J. Pedlosky, 1998: Barotropic circulation around islands with friction. *J. Phys. Oceanogr.,* **28,** 2148–2162.

Radko, T., 1997: Theoretical studies in mesoscale jets and vortices. Ph.D. dissertation, The Florida State University, 129 pp.

Rintoul, S. R., 1991: South Atlantic interbasin exchange. *J. Geophys. Res.,* **96,** 2675–2692.

Saunders, P. M., and B. A. King, 1995: Oceanic fluxes on the WOCE A11 Section. *J. Phys. Oceanogr.,* **25,** 1942–1958.

Schlitzer, R., 1996: Mass and heat transports in the South Atlantic derived from historical hydrographic data. *The South Atlantic: Present and Past Circulation,* G. Wefer, Ed., Elsevier, 305–323.

Schmitz, W. J., Jr., 1996: On the world ocean circulation. Volume 1: Some global features/North Atlantic circulation. Woods Hole Oceanographic Institute Tech. Rep. WHOI-96-03. [Available from MBL-WHOI Library, Woods Hole, MA 02543.]

Semtner, A. J., and R. M. Chervin, 1988: A simulation of the global ocean circulation with resolved eddies. *J. Geophys. Res.,* **93,** 15 502–15 522.

Shannon, L. V., 1985: The Benguela ecosystem. I. Evolution of the Benguela, physical features and processes. *Oceanography and Marine Biology. An Annual Review,* M. Barnes, Ed., University Press, 105–182.

Stramma, L., and R. J. Peterson, 1990: The South Atlantic Current. *J. Phys. Oceanogr.,* **20,** 846–859.

Toggweiler, J. R., and B. Samuels, 1993: Is the magnitude of the deep outflow from the Atlantic Ocean actually governed by southern hemisphere winds? *The Global Carbon Cycle,* M. Heimann, Ed., NATO ASI Series, Vol. 1, Springer-Verlag, 303–331.

——, and ——, 1995: Effect of Drake Passage on the global thermohaline circulation. *Deep-Sea Res.,* **42,** 477–500.

van Ballegooyen, R. C., M. L. Gründlingh, and J. R. E. Lutjeharms, 1994: Eddy fluxes of heat and salt from the southwest Indian Ocean into the southeast Atlantic Ocean: A case study. *J. Geophys. Res.,* **99,** 14 053–14 070.

Veronis, G., 1973: Model of world ocean circulation, I. Wind-driven, two layer. *J. Mar. Res.,* **31,** 228–288.

Whitworth, T., III, and W. D. Nowlin Jr., 1987: Water masses and currents of the southern ocean at the Greenwich Meridian. *J. Geophys. Res.,* **92,** 6462–6476.

Zalesak, S. T., 1979: Fully multidimensional flux-corrected transport algorithms for fluids. *J. Comput. Phys.,* **31,** 335–362.